Available online at www.sciencedirect.com
SCIENCE DIRECT®
European Journal of Mechanics B/Fluids 23 (2004) 727–736

Regeneration mechanism of streaks in near-wall quasi-2D turbulence

M.F. Baig *, S.I. Chernyshenko

School of Engineering Sciences, University of Southampton, Highfield, Southampton SO17 1BJ, UK

Received 27 June 2003; accepted 6 February 2004

Available online 15 April 2004

Abstract

A direct numerical simulation of quasi-2D (that is with flow variables independent of streamwise direction) decaying and forced turbulent flow in a channel was performed in order to seek out the sustenance mechanism of near-wall turbulence by uncovering the mechanism of streak formation. We found the existence of streaks in quasi-2D turbulent flows, thereby demonstrating that feedback from longitudinal flow is not necessary for streak formation. Passive scalars having different mean profiles were introduced in forced quasi-2D turbulent flows in order to compare the streak spacing of the scalars deduced from two-point correlations of DNS results with those obtained from optimal perturbation and Reynolds normal stress anisotropy instability mechanisms. It has been found that although for all the passive scalars the vortex structure is the same, there is a marked variation in streak spacing of the scalars implying that the preferential streak spacing is not necessarily linked to the preferential vortex spacing.

Keywords: Streak spacing; Quasi-2D forced turbulence; Reynolds normal stresses anisotropy; Optimal perturbations; Passive scalars

1. Introduction

The near-wall organised structures are dominated by the presence of quasi-streamwise vortices and streaks. These streaks are sinuous arrays of alternating high and low-speed streamwise jets approximately 1000 wall units long with an average spanwise wavelength of 100 wall units [1]. The quasi-streamwise vortices are roughly 200 wall units long [2] and lie above and adjacent to the streaks. The major fact known about near-wall turbulence is that it is sustained through a continous cycle of generation and break-down of these coherent structures which also leads to development of turbulent skin-friction drag [3]. We know that for turbulence to sustain itself, vortex formation must recur. Several regeneration mechanisms have been proposed and they can be broadly classified under two headings namely the direct induction of existing vortices ('parent-offspring' scenario) or the recurring instability of a quasi-steady base flow. There is a considerable disagreement regarding the nature of instability among the various instability-based theories such as direct resonance of oblique modes [4], lateral waves instability [5], shear-driven instability [6], streak instability without any parent vortex [7]. All these theories essentially imply 3D mechanism, so that the feedback from longitudinal flow to the cross-flow is crucial.

There are two theories, however, where the streaks are formed from a chaotic background even in the absence of feedback from the longitudinal flow direction. One is the optimal perturbation (OP) theory proposed by Butler and Farrell [8] based on linearized Navier–Stokes equations. The optimal perturbations are those perturbations which attain maximal energy growth

* Corresponding author
E-mail addresses: m.f.baig@soton.ac.uk (M.F. Baig), s.chernyshenko@soton.ac.uk (S.I. Chernyshenko).
URL: http://www.afm.ses.soton.ac.uk (S.I. Chernyshenko).

0997-7546/$ – see front matter
doi:10.1016/j.euromechflu.2004.02.004

in time not greater than the eddy-turnover time. These optimal perturbations turn out to be longitudinal vortices [8] which then create the streaks by the lift-up mechanism. The other theory [9] explains the formation of longitudinal vortices as a result of instability caused by the Reynolds normal stress anisotropy (RNSAI) mechanism. This theory utilises the well-known anisotropy of near-wall flows, namely the non-zero difference $Q = \langle v'^2 - w'^2 \rangle$ of Reynolds stresses in spanwise and wall-normal directions. The derivative of Q in wall-normal direction plays the role of buoyancy force creating an instability akin to Rayleigh–Benard instability. This instability has been analysed mathematically using simple passive-admixture transport equation for the Reynolds-stress perturbations. It was found that the fastest growing eigensolutions describe longitudinal vortices [9]. Both theories, when applied to a usual turbulent near-wall flow, predict the correct streak spacing.

In the present study we aim to check the various regeneration theories and find out the dominant mechanism responsible for generation of streaks. By performing calculations of quasi-2D flows, i.e., flows which have all the dynamical variables independent of longitudinal coordinate x, we aim to distinguish between RNSAI and OP on one hand and all the heories that rely on three-dimensionality of the flow on the other hand. Further by introducing passive scalars with different mean scalar profiles in randomly forced quasi-2D turbulence we wish to compare streak spacing of the scalars using both two-point spanwise correlations and predictions from OP and RNSAI theories.

2. Decaying quasi-2D turbulence

Flow in a plane channel is considered. The channel walls are at $z = \pm 1$. Initial conditions of mean turbulent streamwise velocity profile with no perturbations and random cross-flow velocity perturbations that generate isotropic eddies have been imposed. The initial conditions and, hence, the entire solution are assumed to be independent of the longitudinal coordinate, x. Since $\partial/\partial x = 0$ the modified continuity and momentum equations become:

$$\frac{\partial v}{\partial y} + \frac{\partial w}{\partial z} = 0, \tag{1}$$

$$\frac{\partial u}{\partial t} + v\frac{\partial u}{\partial y} + w\frac{\partial u}{\partial z} = -\frac{\partial p}{\partial x} + \frac{1}{\mathrm{Re}}\nabla^2 u, \tag{2}$$

$$\frac{\partial v}{\partial t} + v\frac{\partial v}{\partial y} + w\frac{\partial v}{\partial z} = -\frac{\partial p}{\partial y} + \frac{1}{\mathrm{Re}}\nabla^2 v, \tag{3}$$

$$\frac{\partial w}{\partial t} + v\frac{\partial w}{\partial y} + w\frac{\partial w}{\partial z} = -\frac{\partial p}{\partial z} + \frac{1}{\mathrm{Re}}\nabla^2 w, \tag{4}$$

where $\partial p/\partial x = -1$. The boundary conditions are no-slip for the walls, i.e., $\mathbf{u} = 0$ and periodic in spanwise and streamwise directions. It can be seen that the cross-flow equations do not involve the longitudinal velocity u, that is v and w are governed by the 2D continuity and Navier–Stokes equations (1), (3) and (4). For the initial conditions, a random eddy model has been constructed, in which the streamwise component u is given by mean turbulent streamwise velocity profile with no perturbations, while v and w are given as

$$v(y,z) = -A\sum_{i=1}^{N}(-1)^i \frac{(z-z_i)}{a_i^2} h(\tilde{r}), \tag{5}$$

$$w(y,z) = A\sum_{i=1}^{N}(-1)^i \frac{(y-y_i)}{a_i^2} h(\tilde{r}), \tag{6}$$

where A is the amplitude by which we can increase or decrease the magnitude of the random velocity perturbations, N is the number of randomly generated eddies, y_i and z_i are the coordinates of the centers of the eddies, and $\tilde{r}$ and $h(\tilde{r})$ are given by

$$\begin{aligned} &\tilde{r} = \sqrt{\frac{(z-z_i)^2}{a_i^2} + \frac{(y-y_i)^2}{a_i^2}}, \\ &h(\tilde{r}) = 0, \quad \tilde{r} \geqslant 1, \\ &h(\tilde{r}) = \mathrm{e}^{-1/(\tilde{r}-1)^2}, \quad \tilde{r} \leqslant 1. \end{aligned} \tag{7}$$

In order to have a homogeneous random distribution of eddies in the spanwise direction, we assume $y_i = f(\zeta,\eta) = L_y\zeta$ where L_y is the spanwise length of the computational box and ζ are the random numbers generated based on uniform deviates which lie within a range of (0 to 1). Similarly, a non-homogeneous random distribution of eddies in wall-normal direction is attained using $z_i = g(\zeta,\eta) = \cos(\pi\eta)$, where η are the random numbers uniformly distributed lie within the same range of (0 to 1).

This distribution gives a larger concentration of eddies near the walls at $z = \pm 1$. The probability density function $\rho(y, z)$ of the distribution of random eddies in two-dimensional space is given by the relation [10]

$$\rho(y_i, z_i) = \tilde{\rho}(\zeta, \eta) J^{-1} = \frac{1}{L_y f'(\eta)} = \frac{1}{L_y \pi \sin(\pi \eta)}, \tag{8}$$

where J is the Jacobian $\left| \begin{smallmatrix} g_\zeta & g_\eta \\ f_\zeta & f_\eta \end{smallmatrix} \right|$.

From the definition of number density, we can relate $\rho(y, z)$ and the mean distance l between the centers of N randomly generated eddies as

$$l = \frac{K}{\sqrt{\rho(y, z) N}}, \tag{9}$$

where K is a constant. We have taken the eddy radius $a_i = l(y_i, z_i)$. The eddies which overlap with the walls are neglected. That is if $|z_i - 1| \leqslant a_i$, or $|z_i + 1| \leqslant a_i$, the corresponding term is not added to Eqs. (5) and (6). The no-slip boundary conditions are imposed at the walls for all the velocity components.

2.1. Formation of streamwise streaks

The numerical experiments have been performed in a computational box of size $L_x = 0.005$, $L_y = 6.0$ and $L_z = 2.0$ on a grid having 4*480*480 nodal points at a $\mathrm{Re}_\tau = 180.0$ using a pseudo-spectral parallel code of Sandham and Howard [11] on the Linux Beowulf cluster. The Fourier transform was performed on the velocity field equations (5), (6), and Fourier modes corresponding to the fifty highest and fifty lowest wavenumbers were excluded and then inverse Fourier transformation was performed to get the velocity field initial condition. The resulting flowfield did not contain any wavelength above 0.1, while the span-wise length $L_y = 6.0$. The simulations have been performed for a maximum non-dimensional time of 0.4 at a constant amplitude $A = 4.0$ with $N = 5000$ eddies corresponding to an initial cross-flow Reynolds number $\mathrm{Re}_{\mathrm{cf}} = 305$ based on mean kinetic cross-flow velocity. The temporal development of the low-speed streaks can be seen from the fluctuating negative streamwise velocity contours as shown in Fig. 1, corresponding to non-dimensional times 0.05 and 0.4. It can be seen that the

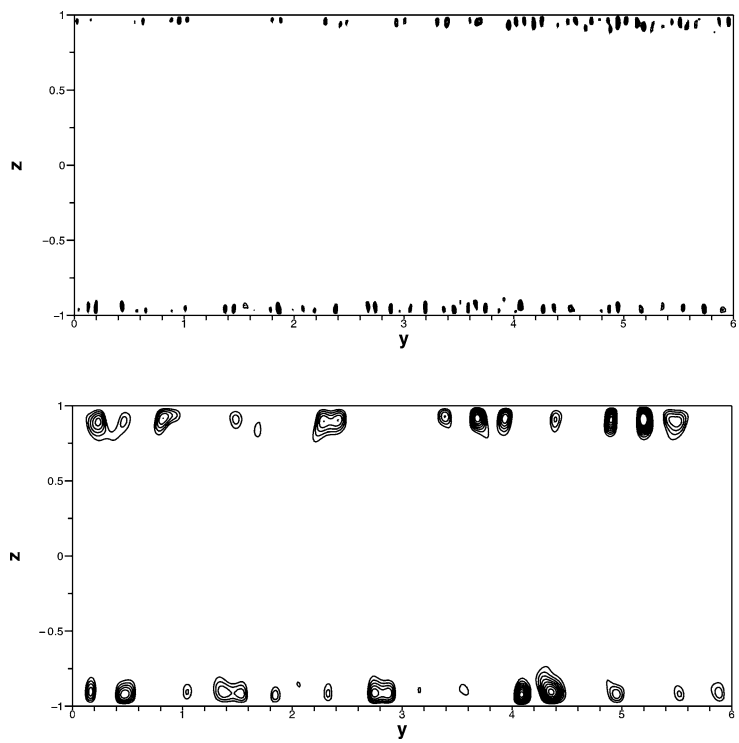

Fig. 1. Streamwise fluctuating velocity u' showing low-speed streaks at time in stants 0.05 (top) and 0.4. Black areas are where $u' < 0.25$ of minimum negative u'.

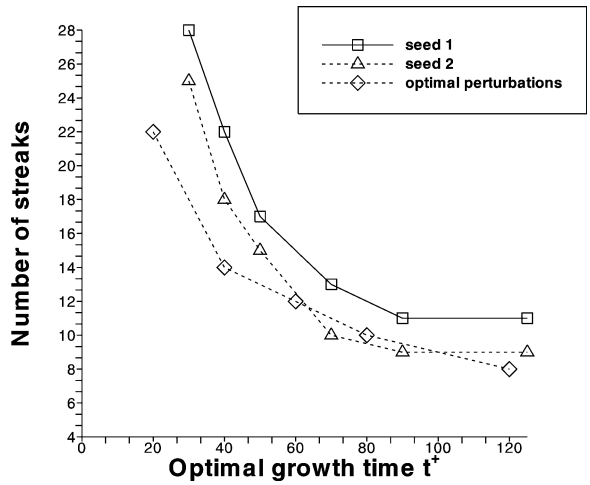

Fig. 2. Comparison of number of streaks for two different realizations of decaying quasi-2D turbulence with streaks computed based on optimal perturbation theory [8].

streaks start forming near the walls after a non-dimensional time $t = 0.03$ and by the time $t = 0.05$ they have lifted off and reached $z = 0.1$. It has been found that for all the time duration, approximately 12–14 low-speed streaks form near the walls.

From analysis of the evolution of the power spectrum it was found that there is a shift of energy from high to low-wavenumbers but there is no selection of particular wavelength during the initial stages. Since initially the energy of the modes with low wavenumbers was exactly zero, this shift has to be due to an inverse energy cascade. The profile of $Q = \langle v'^2 - w'^2 \rangle$ has been computed at different wall-normal distances and time instances, and though the profile near the walls exhibits a behaviour which can lead to a transient RNSAI, no comparison with RNSAI theory can be made as the mean flow is time-dependent. Therefore, the observed behaviour can be described as an initial non-linear inverse energy cascade in the cross-flow, followed by a decay governed by linearized equations. Fig. 2 shows a comparison of number of streaks as a function of time as predicted by optimal perturbation theory (the data from [8]) with the number of streaks observed in our calculations using velocity auto-correlations. The velocity auto-correlation function $R_{uu}(\Delta, z) = \langle u(t, x, y, z)u(t, x, y + \Delta, z)\rangle$ has a maxima at $\Delta = 0$ and reaches a minimum at a certain value Δ_0. Streak spacing can be defined as $2\Delta_0$ and has been used to compute the number of streaks. The curves identified as seed 1 and seed 2 in the figure refer to two different realizations of the flow for two different random number generator seeds.

3. Passive scalar admixture streaks

Passive scalar admixture concentration θ is governed by the equation

$$\frac{\partial\theta}{\partial t} + v\frac{\partial\theta}{\partial y} + w\frac{\partial\theta}{\partial z} = S(z) + \frac{1}{\mathrm{Re}\,Sc}\nabla^2\theta \tag{10}$$

where $S(z)$ is the source term for the passive scalar and Sc is the Schmidt number. For any given mean profile of θ, the same lift-up mechanism which produces the velocity streaks, also produces 'admixture streaks'. We have modified the pseudo-spectral channel code of [11], in order to solve an arbitrary number of passive-scalar equations simultaneously with the momentum equations. Similar to velocity auto-correlation being used to compute streak spacing, auto-correlation for the passive admixture concentrations can be used for determining the admixture streak spacing. Since the equations for the admixture concentration are linear, a linear combination of several solutions is a solution. If $\theta = \sum_{i=1}^{i=n} A_i\theta_i$ then the averaged profile $\bar{\theta}$ and auto-correlation $R_{\theta\theta}$ are given as

$$\begin{aligned}\langle\theta\rangle &= \sum_{i=1}^{i=n} A_i\langle\theta_i\rangle,\\ R_{\theta\theta}(\Delta) &= \sum_{i=1,\,j=1}^{i=n,\,j=n} A_iA_jR_{\theta_i\theta_j}(\Delta).\end{aligned} \tag{11}$$

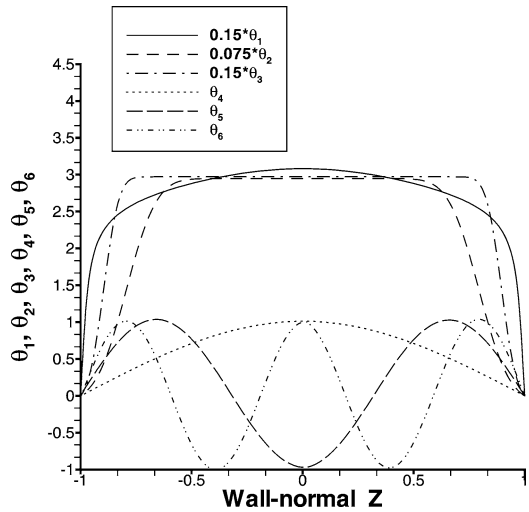

Fig. 3. Statistically averaged and spline-interpolated Q vs z profile from DNS of forced quasi-2D turbulence.

Here Δ is the separation distance in the spanwise direction y. Therefore, by solving simultaneously several passive admixture equations with different source terms and calculating the cross-correlations $R_{\theta_i\theta_j}(\Delta)$ it is possible to compute auto-correlation and, hence, the streak spacing, for any linear combination determined by the vector of coefficients A_i. The linear combination technique can then be used to regulate the streak spacing by varying the mean admixture profile. We determine the new scalar profile by the vector $(A_1, \ldots, A_n)$ such that the corresponding auto-correlation function is as small as possible at a specific value of $\Delta = \Delta_0$. This leads to a minimisation problem for the functional

$$\sum_{i=1,\,j=1}^{i=n,\,j=n} A_i A_j [R_{\theta_i\theta_j}(\Delta_0) - \lambda\delta_{i,j}] \to \min, \tag{12}$$

where λ is the Lagrange multiplier for the fixed norm of initial conditions and $\delta_{i,j}$ is the Kronecker delta. This, in turn, can be reduced to a linear eigenvalue problem. This method has been used to obtain passive admixture profiles with quite large and quite small streak spacings by varying Δ_0.

Six basic admixture mean profiles were calculated. The first three profiles are similar to shapes expected in turbulent flows while the three other profiles are trigonometric functions. The profiles we used are defined via their derivatives with respect to z. Introducing two auxiliary functions,

$$g(z, \mathrm{Re}) = 0.5\left(1 + \left(0.525\frac{\mathrm{Re}}{3}\left(1 + z^2 - 2z^4\right)\left(1 - \mathrm{e}^{-(1-|z|)\,\mathrm{Re}/37}\right)^2\right)^{0.5} - 0.5\right), \tag{13}$$

where $g(z, \mathrm{Re})$ is the Reynolds–Tiederman profile used by Waleffe and Kim [12], and

$$h(z, d, w] = 150\left(\mathrm{e}^{-(-1+d-z)^2/w^2} - \mathrm{e}^{-(-1+d+z)^2/w^2}\right) \tag{14}$$

the derivatives of the basic mean profiles are

$$\bar{\theta}_1' = -z \times \mathrm{Re}/\left(1 + g(z)\right), \quad \bar{\theta}_2' = h(z, 0.2, 0.150), \quad \bar{\theta}_3' = h(z, 0.1, 0.075),$$
$$\bar{\theta}_4' = \sin\left(1 \times \pi(1+z)/2\right), \quad \bar{\theta}_5' = \sin\left(3 \times \pi(1+z)/2\right), \quad \bar{\theta}_6' = \sin\left(5 \times \pi(1+z)/2\right).$$

Fig. 3 shows the statistically averaged wall-normal variation of mean scalar profiles $\bar{\theta}_1$ to $\bar{\theta}_6$.

4. Quasi-2D forced turbulence

The numerical experiments were carried out by subjecting quasi-2D turbulent flows to statistically steady-state forcing using random amplitude body force terms in the governing Navier–Stokes equations. It is not critical whether deterministic or stochastic forcing is applied to sustain quasi-2D turbulence [13]. The initial conditions are the same as mentioned above for 2D decaying turbulence. The body forces **f** have been added to Eqns. (l)–(4) and they have random variation of amplitude (with

a zero mean) in time, a sinusoidal spatial variation of fixed wavenumbers (l, k) in spanwise and wall-normal directions and a peaked near-wall amplitude in wall-normal direction $\zeta(z)$. In order to generate peaked near-wall forcing which reduces to zero towards the centre of the channel, various functions $\zeta(z)$ have been used ranging from an approximation of the Dirac delta to two-hump functions. The forces are then given as

$$\begin{aligned} f_x &= 0.0, \\ f_y &= A(w_f t)\cos\left(\frac{2\pi l y}{L_y}\right)\zeta(z)\cos\left(\frac{2\pi k z}{L_z}\right), \\ f_z &= -\int_{-1}^{z} f_y' \,\mathrm{d}z \end{aligned} \tag{15}$$

that is a divergence-free body force was applied. Here $\zeta(z) = (1 - |z|)\,\mathrm{Re}(\mathrm{Re}\,|z|)^n$ approximates a two-hump function of magnitude O(1) with its width controlled by a factor n. The numerical simulations were performed at $\mathrm{Re} = 360$ on a $4 \times 256 \times 160$ mesh for $n = 8$ with a fixed spanwise mode $l = 55$, wall-normal mode $k = 1$, amplitude $A = 0.05$ and a forcing frequency $w_f = 100$ in terms of non-dimensional time. The forcing of the flow leads to forcing sustained turbulence by the time $t = 25.0$. The flag is then turned on to perform statistical averaging and the statistics are gathered for a very long time until $t = 330.0$.

Then we apply the theory [9] to the case in question. This amounts to the linear stability analysis of the ensemble-averaged two-dimensional Navier–Stokes equations in a cross-flow (y–z) plane together with the passive-admixture equations providing the closure for the Reynolds-stress perturbations. The resulting linearized perturbation equations are written in the following form (see [9]):

$$\frac{\partial \widetilde{w}}{\partial t} = -\frac{\partial \widetilde{\Pi}}{\partial z} + \frac{1}{\mathrm{Re}}\nabla^2 \widetilde{w} + \frac{\partial \widetilde{Q}}{\partial z} - \frac{\partial \tilde{\tau}}{\partial y}, \tag{16}$$

$$\frac{\partial \tilde{v}}{\partial t} = -\frac{\partial \widetilde{\Pi}}{\partial y} + \frac{1}{\mathrm{Re}}\nabla^2 \tilde{v} - \frac{\partial \tilde{\tau}}{\partial y}, \tag{17}$$

$$\frac{\partial \tilde{v}}{\partial y} + \frac{\partial \widetilde{w}}{\partial z} = 0, \tag{18}$$

$$\frac{\partial \widetilde{Q}}{\partial t} + \widetilde{w}\frac{\partial \overline{Q}}{\partial z} = \frac{1}{\mathrm{Re}}\nabla\big(E\nabla \widetilde{Q}\big), \tag{19}$$

$$\frac{\partial \tilde{\tau}}{\partial t} = \frac{1}{\mathrm{Re}}\nabla(F\nabla\tilde{\tau}). \tag{20}$$

Here tildes denote the fluctuating quantities, E and F are turbulent-to-laminar viscosity ratios, which for simplification we have considered as equal to one. Here the modified pressure $\Pi = p + \langle v'^2 \rangle$ while Reynolds shear stress $\tau = \langle v'w' \rangle$. Further modifications of the fluctuations to the harmonic wave form leads to the following system of equations:

$$\begin{aligned} &\frac{1}{\mathrm{Re}}\left(\frac{\imath}{\alpha}\frac{\mathrm{d}^4\widehat{w}}{\mathrm{d}z^4} - 2\alpha\imath\frac{\mathrm{d}^2\widehat{w}}{\mathrm{d}z^2} + \imath\alpha^3\widehat{w}\right) - \imath\alpha\frac{\mathrm{d}\widehat{Q}}{\mathrm{d}z} = \Lambda\left(\frac{\imath}{\alpha}\frac{\mathrm{d}^2\widehat{w}}{\mathrm{d}z^2} - \imath\alpha\widehat{w}\right), \\ &\frac{1}{\mathrm{Re}}\left(\alpha^2\widehat{Q} - \frac{\mathrm{d}^2\widehat{Q}}{\mathrm{d}z^2}\right) + \widehat{w}\frac{\mathrm{d}\widehat{Q}}{\mathrm{d}z} = -\Lambda\widehat{Q}, \\ &\widehat{w} = \widehat{Q} = \frac{\mathrm{d}\widehat{w}}{\mathrm{d}z} = 0 \quad \text{at } z = \pm 1. \end{aligned}$$

Here, α is the spanwise wavenumber, Λ is the circular frequency, $\widehat{w}$ and $\widehat{Q}$ are the amplitude of perturbations in the wall-normal velocity and difference of Reynolds normal stresses. The above system of equations has been discretized using fourth-order accurate finite difference scheme and formulated as an eigenvalue problem. The stability code has been validated by comparing our results with Nikitin's [9] results. From the DNS of quasi-2D forced turbulence, we have extracted a time and space-aver aged profile of Q vs. z and achieved a resonably good behaviour of Q near the walls, but it remained, in contrast to natural 3D flows, far from zero in the center of the channel. The averaged Q profile has been smoothed by using exponential decay of near-wall peaks to constant zero values away from the walls and then a cubic spline interpolation [14] has been used to generate the profile used for RNSAI calculations (see Fig. 4).

Using the eigenvalue solver we computed the maximum unstable eigenvalues σ which display the growth rate of streamwise vortices and we get the maximum diameter (size) of the streamwise vortices at λ_y^+ approximately equal to 155 wall units. The wall units are arbitrary units of measure in our quasi-2D flows because in the cross-flow plane the longitudinal flow is of no

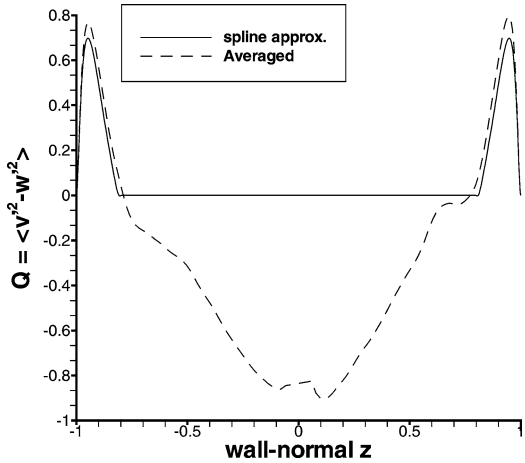

Fig. 4. Statistically averaged variation of six basic mean scalar profiles $\bar{\theta}_i$.

importance and therefore wall-friction velocity u_τ is an irrelevant parameter to cross-flow (y–z) plane. We prefer, however, to use the wall units because they provide a reference frame for comparison of results and also it is a standard practice to measure the streak spacing in wall units. As per the phenomenological model of lift-up mechanism in which two quasi-streamwise vortices flank each high or low-speed streaks, we get a streak spacing of 310 wall units for all the passive scalars.

We then used the technique described above to obtain new profiles using linear combinations of the basic six passive scalar profiles such that we get streak spacing as twice the location Δ of the first minima of two-point correlations [15] of new profiles θ_{ni}. The new five profiles θ_{ni} which have increasing streak spacing (λ_y^+ from 90, 210, 470, 945 to 1515) are shown in Fig. 5. It can be seen from Figs. (5a)–(5e) that as the profile shapes change, with the "shear zone" progressively shifting away from the wall towards the centre of the channel, the two-point correlations attain their minima at larger spanwise distances, indicating a continual growth of streak spacing. This increase of spanwise streak spacing can be also visualized from the accompanying Figs. (5a)–(5e) of low-speed streaks shown in cross-flow (y–z) planes. It is apparent from Figs. (5a)–(5e) that the number of streaks reduces from approximately 20 to 2 as we move down from profile θ_{n1} to θ_{n5}.

5. Nonmodal analysis

The next logical step is to compute the optimal wavelengths for the new scalar profiles θ_{ni} using the optimal perturbation mechanism. The mathematical formulation involves solving two-dimensional linearized Navier–Stokes equations in the cross-flow y–z plane as given by Eqs. (16)–(18). These can be transformed to linearized vorticity–streamfunction formulation by taking the curl of Eqs. (16), (17). On further assuming the streamfunction and vorticity perturbations satisfy the harmonic wave form

$$\begin{aligned} \psi' &= \mathrm{e}^{(\imath\alpha y - \Lambda t)} f(z), \\ w' &= \mathrm{e}^{(\imath\alpha y - \Lambda t)} \widehat{w}(z) \end{aligned} \tag{21}$$

the linearised streamfunction–vorticity equations take the form

$$\alpha^4 f(z) - 2\alpha^2 f''(z) + f''''(z) = \mathrm{Re}\,\Lambda\left(\alpha^2 f(z) - f''(z)\right) \tag{22}$$

with the boundary conditions

$$f(\pm 1) = 0, \quad \frac{\mathrm{d}f}{\mathrm{d}z}(\pm 1) = 0. \tag{23}$$

Here $f(z)$ is the amplitude of streamfunction perturbations, Λ is the circular frequency and α is the spanwise wavenumber. The linearized source equation governing the development of longitudinal flow is given as

$$\frac{\partial u'}{\partial t} + w' \frac{\mathrm{d}U}{\mathrm{d}z} = \frac{1}{\mathrm{Re}} \nabla^2 u'. \tag{24}$$

Here U is the mean streamwise velocity profile while u' and w' are streamwise and wall-normal velocity perturbations. The above mentioned equations (21)–(24) are solved using the eigenfunction expansion approach [16] while taking the

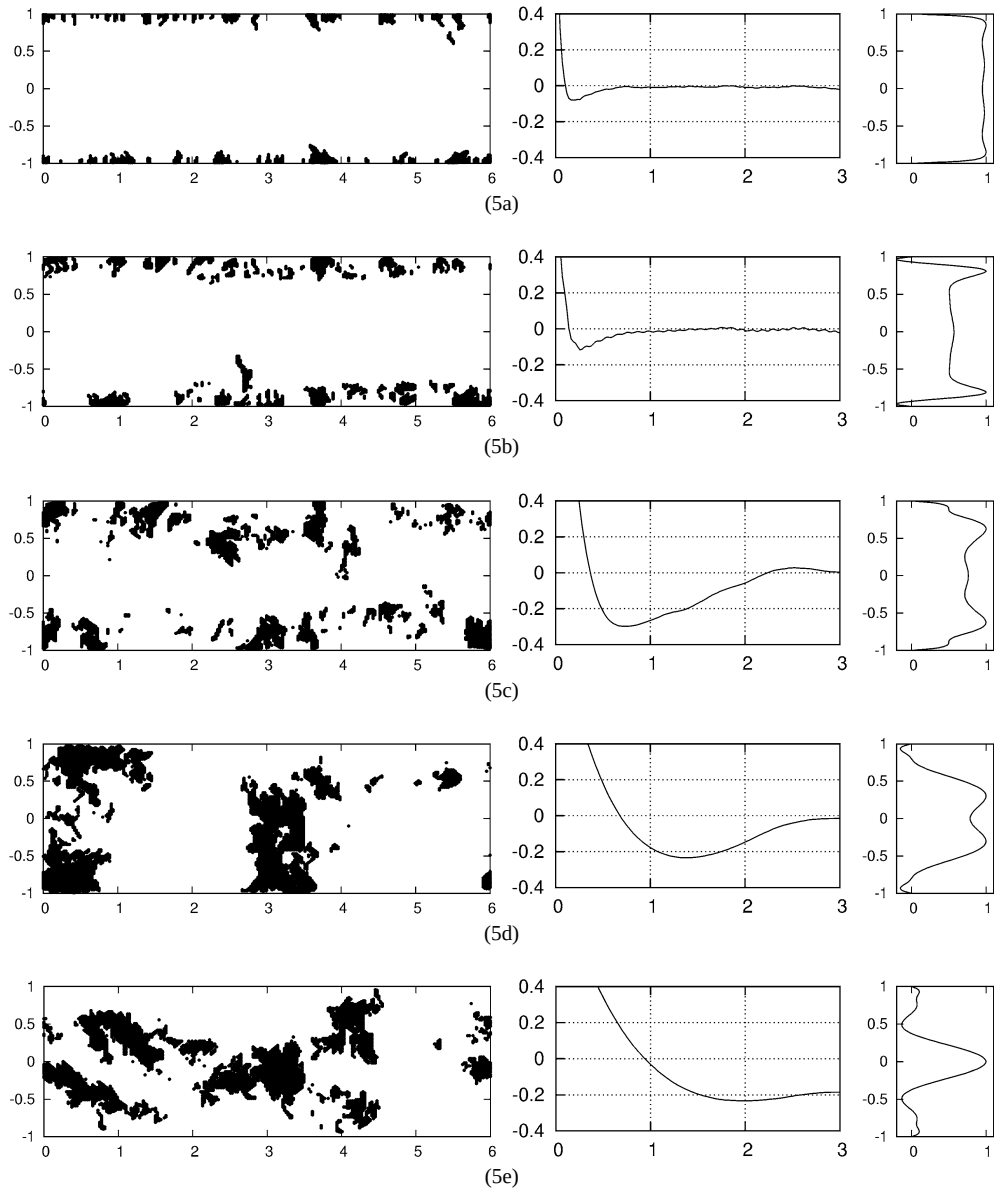

Fig. 5. New mean scalar profiles $\bar{\theta}_{ni}$ generated using linear combination of basic profiles, their two-point autocorrelation functions and streamwise fluctuating u' contours showing increased streak spacing.

assumption that optimal perturbations are independent of the longitudinal coordinate [8]. The computer code has been verified by reproducing the results from the paper of Butler and Farrell [8].

We have computed optimal perturbations for all the five new mean profiles θ_{ni} using the approach followed by Butler and Farrell [8]. In their approach, a linear perturbation grows undisturbed for an unlimited time in a laminar flow, but in turbulent flow the development is disrupted by small-scale turbulent motions. The time scale that characterises this disruption is the eddy turnover time τ_e, the ratio of the square of the characteristic turbulent kinetic energy, $q^2 = \overline{u_i u_i}$, to the dissipation rate $\varepsilon = \nu \overline{u_{i,j} u_{i,j}}$ and hence the optimal disturbance development should be regulated by a time interval consistent with eddy turnover time near the wall. In Fig. 6, non-dimensional eddy turnover time τ_e has been obtained after performing long time-averaged statistics and is plotted as a function of distance from the wall. For the new scalar profile θ_{n2}, at five optimization times representative of the eddy turnover time near the wall, optimal energy growth has been computed as a function of spanwise wavelength λ_y^+ and plotted as shown in Fig. 7.

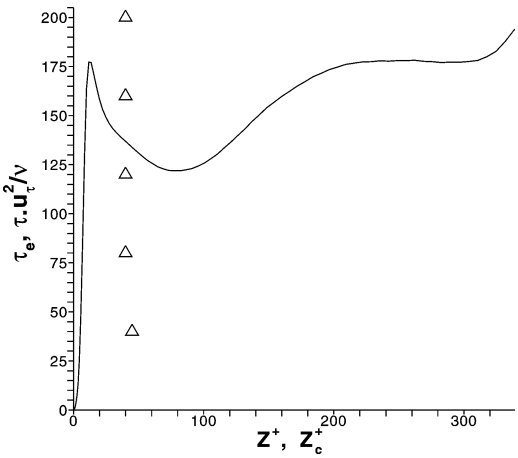

Fig. 6. Eddy turnover time τ_e versus distance from the wall (—). Also plotted (Δ) is optimal growth time τ^+ versus location of peak scalar perturbation, z_c^+ at optimal times $t = \tau^+$, for the new scalar profile θ_{n2}.

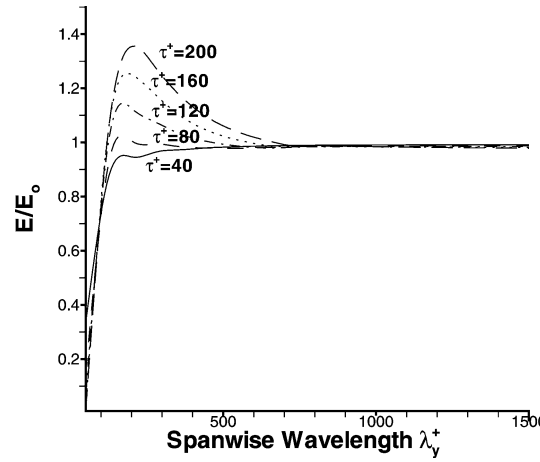

Fig. 7. Optimal energy growth versus wavelength for optimization times representative of the eddy turnover time for the new scalar profile θ_{n2}.

Table 1
Comparison of streak spacing from DNS results of two-point correlations of randomly forced quasi-2D turbulence with predictions from RNSAI [9] and OP [8] theories

Scalar	Streak spacing from DNS	Streak spacing from RNSAI [9]	Streak spacing from OP [8]
θ_{n1}	90	310	120
θ_{n2}	210	310	200
θ_{n3}	470	310	220
θ_{n4}	945	310	280
θ_{n5}	1515	310	350

Corresponding to these optimization times τ^+, particular wavelengths λ_y^+ can be computed where energy growth E/E_0 is maximal. Knowing τ^+ and λ_y^+, i.e., fixing the eigenvalues E/E_0, the corresponding eigenvectors can be computed. The eigenvectors denote the variation of scalar perturbations and from them the wall-normal locations of peak scalar perturbations can be ascertained. These peak scalars corresponding to optimization times of $\tau^+ = 40$, 80, 120, 160 and 200 have their centres located at $z_c^+ = 43$, 40, 40, 40 and 40 respectively and have been plotted as symbols Δ as shown in Fig. 6. The optimization time can be determined by comparing τ^+ as a function of peak scalar location z_c^+ to eddy turnover time as function of z^+, as shown in Fig. 6. The best choice of τ^+ occurs near the intersection of these curves corresponding to $\tau^+ = 135$. This choice produces spanwise streak spacing $\lambda_{\text{streak}} = 200$ wall units.

The same logic has been applied for the other four new profiles and the best choice of τ^+ ascertained by seeking the intersection region in order to get the spanwise streak spacing for each scalar. These results have been tabulated as shown in Table 1.

6. Conclusions

In light of the above results the following conclusions can be drawn:

- Streaks can form even when there is no dependence of flow variables on longitudinal coordinate direction thereby showing that a theory of streak formation need not necessarily rely on three-dimensionality.
- The streak spacing strongly depends on the mean profile even when the vortex structure is fixed. Theories which assume the streak spacing being equal to twice the vortex spacing, like for example, RNSAI theory, cannot explain this fact.
- The only existing theory which describes similar qualitative behaviour is the OP theory by Butler and Farrell [8]. But in many cases the streak spacings observed from our quasi-2D DNS results differ considerably with results from OP theory.

Therefore the good agreement for certain cases, when the mean scalar profile coincides with the mean velocity profile, can be attributed to chance only.

Acknowledgements

This research was supported by EPSRC under the project GR/R27785/01. The first author gratefully acknowledges the School of Engineering Sciences for financial support.

References

[1] C. Smith, S. Metzler, The characteristics of low-speed streaks in the near-wall region of a turbulent boundary layer, J. Fluid Mech. 129 (1983) 27–54.
[2] S. Robinson, Coherent motions in the turbulent boundary layer, Ann. Rev. Fluid Mech. 23 (1991) 601–639.
[3] R. Panton (Ed.), Self-Sustaining Mechanism of Wall-Turbulence, Computational Mechanics, Southampton, 1997.
[4] P.S. Jang, D.J. Benney, R.L. Gran, On the origin of streamwise vortices in a turbulent boundary layer, J. Fluid Mech. 169 (1986) 109–123.
[5] J. Jimenez, P. Moin, The minimal flow unit in a near-wall turbulence, J. Fluid Mech. 225 (1991) 213–240.
[6] J.M. Hamilton, J. Kim, F. Waleffe, Regeneration mechanisms of near-wall turbulence structures, J. Fluid Mech. 232 (1995) 317–348.
[7] W. Schoppa, A. Hussain, Formation of near-wall streamwise vortices by streak instability, in: 29th AIAA Fluid dynamics Conf., Albuquerque, USA, 1998, AIAA 98-3000.
[8] K.M. Butler, B.F. Farrell, Optimal perturbations and streak spacing in wall-bounded turbulent shear flows, Phys. Fluids A 5 (1993) 774–777.
[9] N. Nikitin, S. Chernyshenko, On the nature of organised structures in turbulent near-wall flows, Fluid Dynamics 32 (1) (1997) 18–23.
[10] S. Panchev, Random Functions and Turbulence, Pergamon Press, New York, 1971.
[11] N. Sandham, R. Howard, Direct simulation of turbulence using massively parallel computers, in: D. Emerson, et al. (Eds.), Parallel Computational Fluid Dynamics, North-Holland, 1998.
[12] F. Waleffe, J. Kim, On the origin of streaks in turbulent shear flows, in: 8th Symposium on Turbulent Shear Flows, Springer-Verlag, 1991, paper 5-5.
[13] A. Tsinober, An Informal Introduction to Turbulence, Kluwer Academic, 2001.
[14] W. Press, S. Teukolsky, W. Vellerling, B. Flannery, Numerical Recipes in Fortran, Cambridge University Press, Cambridge, 1992.
[15] J. Kim, P. Moin, R. Moser, Turbulence statistics in fully developed channel flow at low Reynolds number, J. Fluid Mech. 177 (1987) 133–166.
[16] D. Henningson, P. Schmidt, Stability Analysis of Shear Flows, Springer-Verlag, Berlin, 2000.